Effect of electrolyte for back contact transparent conducting oxide-less dye-sensitized solar cells: iodine versus cobalt

Md. Zaman Molla,[a,b,*] **Ajay K. Baranwal**,[a,c] **Shuzi Hayase**,[c] **and Shyam S. Pandey**[a]

[a]Kyushu Institute of Technology, Graduate School of Life Science and Systems Engineering, Kitakyushu, Japan

[b]Ahsanullah University of Science and Technology, Dhaka, Bangladesh

[c]University of Electro-Communications, Info-Powered Energy System Research Center, Tokyo, Japan

Abstract. Grätzel solar cells are reported in a transparent conducting oxide-less (TCO-less) back-contact dye-sensitized solar cell (BC-DSC) architecture using a stainless steel mesh-protected working electrode along with nanoporous TiO_2 semiconductor and metal-free D205 dye. Liquid electrolytes play a significant role for the dye regeneration in the working operation of TCO-less BC-DSCs; therefore, we report the effectiveness of two different commonly utilized electrolytes (iodine- and cobalt-based redox shuttles) for the construction and performance of TCO-less dye-sensitized solar cells (DSCs). Differential performance of DSCs thus fabricated was interpreted utilizing impedance spectral and lifetime analysis. It was found that although utilization of cobalt bipyridyl complex-based electrolyte was able to harvest higher photons in the lower wavelength region (330 to 430 nm) as compared to its iodine electrolyte counterparts, hampered dye regeneration due to reduced driving force and slower ion diffusion in combination with higher charge transport resistance at TiO_2/dye/electrolyte was responsible for relatively hampered photovoltaic performance at peak absorption. [DOI: 10.1117/1.JPE.10.045501]

Keywords: transparent conducting oxide-less; back contact; cobalt/iodine electrolyte; dye-sensitized solar cells.

Paper 20066 received Aug. 3, 2020; accepted for publication Oct. 22, 2020; published online Nov. 9, 2020.

1 Introduction

The breakthrough article produced by Grätzel and O'Regan[1] in 1991 initiated the idea that dye-sensitized solar cells (DSCs) have the ability to convert sunlight into electricity efficiently through light absorption via the dye molecule attached to nanoporous TiO_2. Since then, DSCs have received immense attention owing to their favorable, simple, environmentally friendly fabrication method in combination with good power conversion efficiency surpassing amorphous silicon.[2] Esthetic color and transparency of DSCs make them a potential candidate for building integrated photovoltaic applications.[3] In DSC architecture, an electron-transporting layer TiO_2 printed on the F-doped transparent conductive oxide (FTO) plate holds the monolayer of light-absorbing sensitizer and functions as a working electrode. This working electrode is assembled with a platinum-coated FTO plate (counter electrode) and a redox electron-transporting medium (electrolyte) is inserted to perform the task of dye regeneration. In this traditional architecture of DSCs, the incident photon enters through the FTO and a semiconducting oxide layer (TiO_2); thereafter, the remaining available photon is finally absorbed by the sensitizer. Therefore, a part of the photons would be lost as absorbed or scattered, and will not add up to the photon-induced current of the DSCs. It is estimated that about 20% light is lost in the visible region itself due to FTO glass of the working electrode; moreover, widely used TiO_2 itself shows strong absorption

*Address all correspondence to Md. Zaman Molla, whyzaman@gmail.com

1947-7988/2020/$28.00

around the UV region (300 to 400 nm).[4] Therefore, antireflection coatings have been proposed to substantially reduce the scattered photon loss at the FTO surface.[5] However, these coatings further increase the fabrication steps and overall cost of the DSC. Moreover, the use of two FTO glasses in the fabrication of DSCs makes the architecture even more costly and bulky.[6] Therefore, it is quite necessary to fabricate the DSCs in a robust architecture to boost the photovoltaic performance and minimize the energy payback time while maintaining efficiency.

These issues can be overcome by fabricating DSCs in a structure in which a fully exposed TiO_2 surface is available for photon harvesting, wherein the working electrode and the counter electrode are situated on one side of photoharvesting sensitizer medium. Such back contact DSCs employ a lower number of FTO layers to avoid parasitic optical loss and are proven superior for tandem DSCs applications, where a broad photon spectrum can be harvested.[7] Due to this appealing prospect, they have also been implemented in back contact structures in the state-of-the-art Perovskite solar cells with a reported efficiency of 3.88%.[8] In the first evolution of back contact DSCs, Ti metal mesh was used as an alternative to the FTO working electrode and the photon was incident on semitransparent Pt-coated FTO glass; therefore, this new structure again incurs the loss of photons.[9] In another report, the light was passed through glass holding TiO_2, and Ti metal as a working electrode was deposited by a sputtering method over this semiconducting layer.[10] This structure had a photon advantage and was named transparent conducting oxide-less (TCO-less) DSC. Han et al. discovered the construction of TCO-less DSC architecture, where the porous Ti metal electrode was toward the backside of the device, i.e., opposite to the light irradiation to act as electron collector and therefore named it back-contact (TCO-less) DSC.[11,12] Fu et al.[13] reported back-contact DSCs utilizing microstructured backplates (working and counter electrodes based on FTO plate) positioned below the dye-sensitized heterojunction in a monolithic cell structure. In another report, Bach et al.[14] demonstrated TCO-free monolithic back-contact DSC constructed on flexible Ti foils. Yun et al.[15] reported all TCO-less cost-effective DSC employing Ti and stainless steel (SS)-foil substrates as counter and the working electrode, respectively. Rustomji et al.[16] reported TCO-less DSC with Ti-mesh in a three-dimensional array of TiO_2 nanotubes. Our group reported a TCO-less DSC with a thick and porous Ti electrode and later in order to further reduce the fabrication cost, SS-mesh-based working electrode was employed in the architecture to make it more appealing and lighter.[17,18]

It is very common to observe various studies on performance optimization for TiO_2 layers and dyes in back-contact TCO-less DSCs architecture.[19–23] Although the iodine-based electrolyte shows poor photon absorption in the UV region, the choice between cobalt and iodine electrolyte in these TCO-less DSCs is not yet clear. An electrolyte medium is responsible for charge transport and subsequently, dye regeneration takes place to complete the circuit. The energy gap between the TiO_2 Fermi level and the relevant redox level of the electrolyte decides the open circuit voltage (V_{oc}) of DSC. Since the photoelectric conversion efficiency (PCE) of the photovoltaic cell governs the finally observable V_{oc}, it follows that a suitable choice of the electrolyte may affect and controls the overall functioning of TCO-less back-contact dye-sensitized solar cells (BC-DSCs). In this study, we are presenting the fabrication and characterization of TCO-less BC-DSCs utilizing cobalt and iodine redox shuttles and comparison of their photovoltaic performances employing a metal-free organic indoline D205 dye.

2 Experimental

2.1 *Materials and Methods*

Materials used in this work were purchased commercially and used as received without further purifications. The cobalt complexes tris-(2,2′-bipyridine)cobalt(II) di(hexafluorophosphate) $[Co(bpy)_3(PF_6)_2]$, tris-(2,2′-bipyridine)cobalt(III) tri(hexafluorophosphate) $[Co(bpy)_3(PF_6)_3]$, tris(1,10-phenanthroline)cobalt bis(hexafluorophosphate) $[Co(phen)_3(PF_6)_2]$, and tris(1,10-phenanthroline)cobalt tris(hexafluorophosphate) $[Co(phen)_3(PF_6)_3]$ represented as $[Co(bpy)_3]^{2+}$, $[Co(bpy)_3]^{3+}$, $[Co(phen)_3]^{2+}$, and $[Co(phen)_3]^{3+}$, respectively. In general, the chemical formula of cobalt complexes are $[Co(bpy)_3]^{2+/3+}$ and $[Co(phen)_3]^{2+/3+}$ and used as one electron redox shuttle and were synthesized following previously published paper.[24] Indoline D205 sensitizer

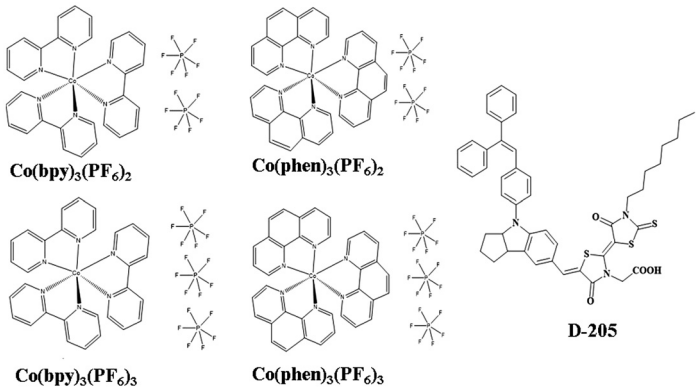

Fig. 1 The chemical structure of the sensitizing dye, cobalt complexes used in the present work.

was bought from Mitsubishi Paper Mills, Japan. Molecular structure of cobalt complexes synthesized and sensitizing dye D205 used in this work are shown in Fig. 1. Thickness of TiO_2 film screen printed over Ti-coated flexible SS-mesh was measured employing a scanning electron microscope (JCM-6000 NeoScope). Electrochemical impedance spectroscopy (EIS) analysis was conducted following the previously published article.[25] Finally, to compare the electron lifetime of TCO-less BC-DSCs utilizing different electrolytes, we carried out open circuit voltage decay (OCVD) (Tektronix TDS2004B) analysis over these devices. The voltage decay with time was utilized for the estimation of electron lifetime.

2.2 *TCO-Less DSC Construction*

TCO-less flexible BC-DSC was constructed employing flexible SS-mesh (SUS-730, Asada Mesh, Japan), wire diameter of 13 μm, and wire spacing of 16 μm. This flexible SS-mesh works both as a current-conducting electrode and a support for the nanoporous TiO_2 film coated onto it. The bare SS-mesh was protected from both sides with a thin layer sputtering (CFS-4EP, Shibaura Mechatronics, Japan) of Ti metal (240 nm) (Ti/SS-mesh) to suppress the back electron reactions from the flexible photoelectrode.[25] We used Ti-Nanoxide (15 to 20 nm) D/SP paste (Solaronix, SA) for screen printing onto the Ti/SS flexible metal mesh, which was sintered at 450°C/30 min. The thickness of the nanoporous TiO_2 film screen printed over the flexible SS-mesh was maintained to be about 11 μm. Flexible photoelectrode was constructed by immersing TiO_2 screen-printed Ti/SS-mesh in the D205 (0.5 mM) solution of *tert*-butanol and acetonitrile (v/v, 1/1) at room temperature for dye adsorption for 16 h. A 60-nm Pt layer was sputtered over an FTO plate to make a counter electrode. To absorb the electrolyte layer, a polytetrafluoroethylene (PTFE: 35-μm thick, H010A293D, ADVANTEC) film was inserted in the middle of the photoelectrode and the platinized TCO counter electrode. The two electrodes viz. working and counter and PTFE film was sandwiched as per the schematic illustration as depicted in Fig. 2 to realize the TCO-less BC-DSC fabricated in this work. To assemble the device, first, a porous PTFE film was placed over the Pt counter electrode. Over this PTFE film, the flexible photoanode (the TiO_2 coated Ti/SS-mesh) is placed. Then a white slide glass from Matsunami glass industries, Japan (S1126) is placed over the top of this flexible photoanode. After electrolyte insertion by a capillary tube, the device was finally sealed using UV-curable resin (3017B, Three Bond corporation, Japan) and smart curing system (ZUV-C20H, Omron, Japan) for UV light irradiation for curing the resin after its application. Cobalt $[Co(bpy)_3]^{2+/3+}$ electrolyte employed in this experiment comprised of (0.22 M) $[Co(bpy)_3]^{2+}$, (0.033 M) $[Co(bpy)_3]^{3+}$, (0.20 M) 4-*tert*-butylpyridine, and (0.1 M) $LiClO_4$ in acetonitrile. The Cobalt $[Co(phen)_3]^{2+/3+}$ electrolyte comprised of (0.22 M) $[Co(phen)_3]^{2+}$, (0.033 M) $[Co(phen)_3]^{3+}$, (0.20 M) 4-*tert*-butylpyridine, and (0.1 M) $LiClO_4$ in acetonitrile. The I^-/I_3^- electrolyte consisted of (0.5 M) LiI, (0.05 M) I_2, (0.58 M) 4-*tert*-butylpyridine, (0.6 M) ethyl-methyl-imidazolium dicyanoimide in acetonitrile.

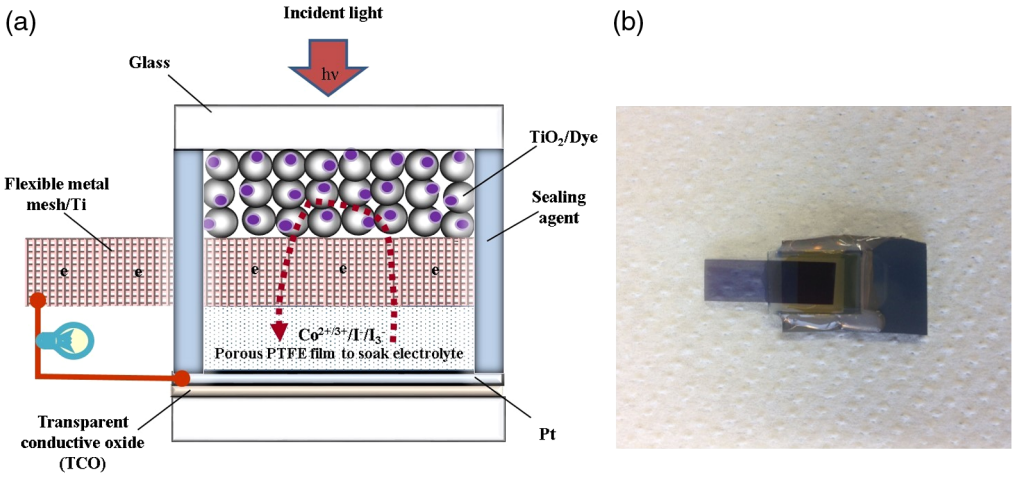

Fig. 2 Schematic cross-sectional view of (a) TCO-less BC-DSC utilizing porous PTFE film as an electrolyte absorber and (b) actual fabricated.

2.3 *Photovoltaic Characterization*

Measurement of the DSC photovoltaic performance was conducted at 100 mW/cm^2 intensity and AM 1.5 condition for all of the devices using a CEP-2000, Bunko Keiki, Japan solar simulator equipped with a xenon lamp (BSO-X150LC, Bunko Keiki). Light exposure in the solar simulator was calibrated using Si photodetector (BS-520 S/N353, Bunko Keiki). The incident photon to current conversion efficiency (IPCE) was carried out in the 300- to 800-nm wavelength region at 1×10^6 photon/cm^2 (photon flux) in DC mode. A metal mask (black) with an opening of 0.2025 cm^2 area was utilized to perform the measurements of the photovoltaic characteristics.

3 Results and Discussion

3.1 *Energy Band Diagram*

Various redox electrolytes can achieve a variable electronic window potential in conjunction with TiO_2 energetics to regenerate the dyes. Here we present the differential performances between cobalt-based electrolyte and the most commonly employed iodine-based electrolyte. The chemical structure of the cobalt electrolyte affects the driving force as well as mass transport. Therefore, variable energetic cobalt redox species of $[Co(bpy)_3]^{2+/3+}$ and a deeper energetic of $[Co(phen)_3]^{2+/3+}$ species were used. Energetic cascade between electron transporting TiO_2 and redox electrolyte is an integral part of the DSC working cycle and it plays a dominant role in deciding their suitability as a sensitizer and controlling the photovoltaic performance. Energy band diagram for DSC utilizing D205 dye and different cobalt and iodine electrolytes are depicted in Fig. 3. To construct energy band diagram, HOMO/LUMO energy level of the dye, conduction band (CB) energy level of TiO_2 semiconductor, and redox energy level of the various electrolytes used for the present work were taken from the literature.[26–28] It is clear from the energy diagram that there is a very large driving force of 0.77 V between the D205 dye LUMO level and CB edge of TiO_2 ensuring the thermodynamic requirement of the electron injection. On the other hand, iodine-based redox electrolyte exhibits a 0.22-V driving force for dye regeneration. Both of the cobalt complex-based redox shuttles exhibit relatively deeper redox potential relative to that of iodine electrolyte imparting the possibility for the attainment of the higher V_{oc}. Concurrently, lowering of redox energy level reduces the driving force of the sensitizer regeneration posing a trade-off between theoretically predicted and experimentally observed V_{oc} values.

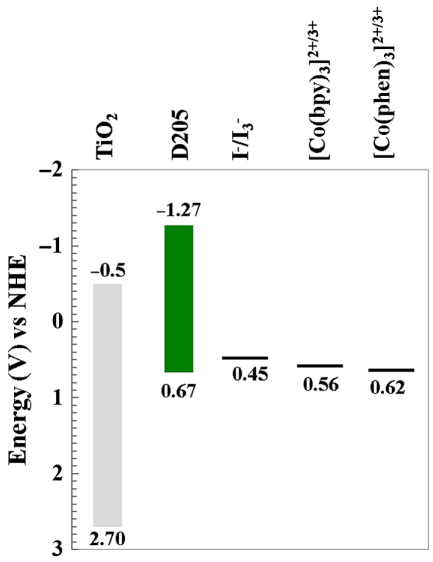

Fig. 3 Energy band diagram for a TiO_2 semiconductor stained with D205 using $[Co(bpy)_3]^{2+/3+}$, $[Co(phen)_3]^{2+/3+}$, and I^-/I_3^--based electrolytes.

3.2 *Effect of Nature of Electrolytes on the Photovoltaic Performance of TCO-Less BC-DSCs Employing Cobalt and Iodine Electrolyte*

According to the energy diagram shown in Fig. 3, the cobalt phenanthroline complex has deeper redox potential compared to the cobalt bipyridine complex, and the cobalt bipyridine complex has deeper redox potential compared to the iodide/tri-iodide complex. The photovoltaic behavior of BC-DSCs utilizing these electrolytes was performed utilizing about 11-μm-thick TiO_2 film in order to investigate the influence of redox potential upon the device performance and the results are presented in Table 1. The V_{oc} usually enhances with a deeper redox potential of the mediators as reported by Devries et al.[29] A similar tendency in voltages was observed in our experiment. The short-circuit current density J_{sc} obtained in the BC-DSCs as shown in Fig. 4 decreases with a more positive redox level of the electrolytes as indicated in the energy diagram (Fig. 3) and Table 1. This decrease in photocurrent density with higher redox potential may be assigned to fast recombination kinetics, slow regeneration processes, and hampered diffusions.[30] These different aspects will be discussed below.

The IPCE measurements were performed for BC-DSCs utilizing D205 sensitizer in combination with $[Co(bpy)_3]^{2+/3+}$, $[Co(phen)_3]^{2+/3+}$, and I^-/I_3^- redox shuttles while maintaining the same (11 μm) TiO_2 thickness. The resulting IPCE spectra are presented in Fig. 5. IPCE with more than 50% value employing I^-/I_3^- electrolyte is observed in the range of 490 to 600 nm. BC-DSCs utilizing $[Co(bpy)_3]^{2+/3+}$ and $[Co(phen)_3]^{2+/3+}$ electrolytes exhibit IPCE value of nearly 40% and more than 20%, respectively, in the range of 390 to 630 nm. From this figure,

Table 1 The photovoltaic results of fabricated TCO-less BC-DSCs measured at 100 mW/cm^2 intensity and AM 1.5 condition using black metal mask having 0.2025 cm^2 opening.

Electrolyte	$[Co(phen)_3]^{2+/3+}$	$[Co(bpy)_3]^{2+/3+}$	Iodide/tri-iodide
Efficiency (%)	1.62 (1.57 ± 0.12)	2.94 (2.89 ± 0.05)	4.18 (4.14 ± 0.05)
FF	0.63 (0.6 ± 0.024)	0.67 (0.67 ± 0.008)	0.75 (0.74 ± 0.006)
V_{oc} (V)	0.74 (0.73 ± 0.005)	0.72 (0.71 ± 0.008)	0.70 (0.70 ± 0.005)
J_{sc} (mA/cm^2)	3.48 (3.59 ± 0.37)	6.04 (6.05 ± 0.006)	7.97 (7.99 ± 0.04)

The values in the bracket denote the mean value of three distinct devices along with standard deviation.

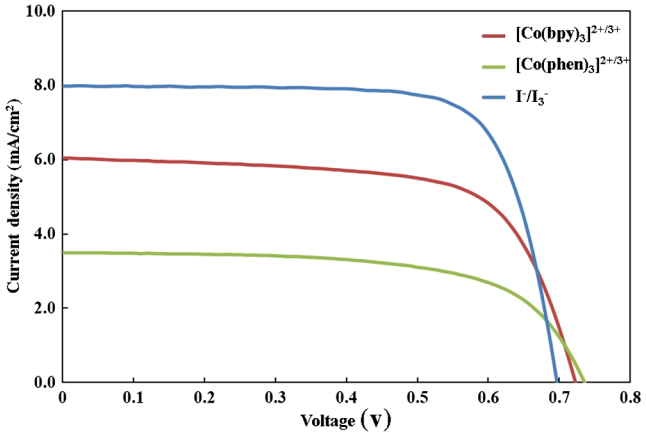

Fig. 4 Current density versus applied potential curves at 100 mW/cm^2 intensity and AM 1.5 condition employing $[Co(bpy)_3]^{2+/3+}$ (red color), $[Co(phen)_3]^{2+/3+}$ (green color), and I^-/I_3^- (blue color) electrolytes.

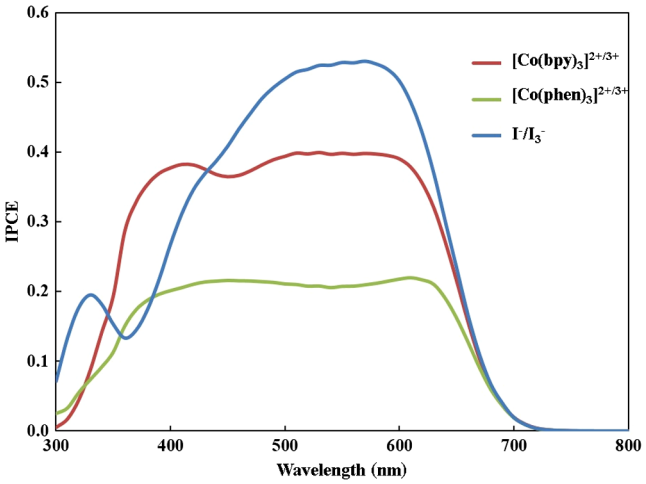

Fig. 5 IPCE action spectra for TCO-less BC-DSCs employing $[Co(bpy)_3]^{2+/3+}$ (red color), $[Co(phen)_3]^{2+/3+}$ (green color), and I^-/I_3^- (blue color) electrolytes.

it is evident that the use of the iodine redox mediator demonstrates the hindered photon harvesting in the visible spectrum of 330 to 430 nm. On the contrary, the $[Co(bpy)_3]^{2+/3+}$ redox mediator shows better photon accumulation in that region. For efficient photovoltaic outcome, the oxidized sensitizer must be regenerated faster before it gets reduced by the CB electrons in the TiO_2. If the regeneration process is not sufficiently fast, it would lead to lower IPCEs. Inadequate regeneration was noted when sensitizers were utilized to widen photon accumulation in the higher wavelength zone of the solar radiation spectrum which led to the insufficient driving force for regeneration.[31,32] It is expected that enhancing the driving force for regeneration must enhance the regeneration rate that means when the overpotential is reduced, the efficient dye regeneration is secured, and that is compatible with the obtained results here. Energy band diagram for DSC utilizing a TiO_2 stained with D205 dye and $[Co(bpy)_3]^{2+/3+}$, $[Co(phen)_3]^{2+/3+}$, and I^-/I_3^--based electrolytes has been shown schematically in Fig. 3. The lower IPCE observed with the $[Co(phen)_3]^{2+/3+}$ complexes may be assigned to a very small driving force for the sensitizer regeneration with a deeper redox potential of the redox shuttle as shown in the energy diagram resulting in very low photocurrent.[32] The redox potential of $[Co(bpy)_3]^{2+/3+}$ and $[Co(phen)_3]^{2+/3+}$ is deeper by 0.11 and 0.17 V, respectively, compared to I^-/I_3^-. The maximum open circuit voltage obtained is resulted from the energy difference

between the TiO_2 Fermi level and the redox energy level of electrolyte used in the operation of DSCs. The deeper redox potential of cobalt electrolyte explains the marginal improvement in V_{oc} in this TCO-less BC-DSCs. Similar results have been reported by Kakiage et al.[33] However, the poor driving force for dye regeneration in cobalt-based electrolyte DSCs, along with the lack of a sufficient number of bulky alkyl group in photo harvesting dye D205, hinders the charge collection efficiency, which is reflected in obtained lower IPCE as well as J_{sc}.[27,33,34]

The OCVD measurements on the BC-DSCs using cobalt- and iodine-based electrolytes were performed to verify that it is in fact recombination that accounts for the variations in IPCE and J_{sc}.[24] The voltage decay data (V_{oc} versus time) were converted to electron lifetime.[35] Since electron lifetime is inversely proportional to the rate of recombination at a given potential, it allows us to have a quantitative comparison.[36] Figure 6 clearly shows that electron recombination is highest for $[Co(phen)_3]^{2+/3+}$ electrolyte among all the cobalt- and iodine-based electrolytes because it has the lowest lifetime at a given potential. As the electron lifetime is highest for iodide/tri-iodide-based electrolyte at a given potential, its recombination rate is lowest among all the electrolytes and shows the highest IPCE and J_{sc} as shown in Figs. 5, 4, and Table 1, respectively.

A number of factors may influence the IPCE and photovoltaic characteristics of DSCs,[37] which creates difficulty in making comparisons with literature results. EIS measurements were conducted to figure out the cause of the differences in the photovoltaic results of BC-DSCs utilizing cobalt and iodine electrolytes. Figure 7 shows the Nyquist plots of BC-DSCs employing $[Co(bpy)_3]^{2+/3+}$, $[Co(phen)_3]^{2+/3+}$, and I^-/I_3^--based redox shuttles. Three semicircles are observed in the measured 5 mHz to 100 kHz frequency range.[38–40] The first semicircle corresponding to high-frequency region (R_1) is associated with the resistance owing to charge transport at the Pt counter electrode. The second semicircle corresponding to mid-frequency region (R_2) is attributed to the resistance due to charge transfer occurring at the TiO_2/dye/electrolyte interface. The third semicircle corresponding to low-frequency region (R_3) corresponds to the resistance because of ion diffusion within the electrolyte. The resistance (1.5 to 5.9 Ω) associated with the first semicircle in the Nyquist plot is associated with the charge transport at the counter electrode, which was not significant determinant for the differential performance of photovoltaic behavior of BC-DSCs utilizing all the $[Co(bpy)_3]^{2+/3+}$, $[Co(phen)_3]^{2+/3+}$, and iodide/tri-iodide-based electrolytes. The charge transport resistance observed at the TiO_2/dye/electrolyte interface for cobalt- and iodine-based electrolytes varies with the increasing order of $[Co(phen)_3]^{2+/3+}$ $[75.53(72.21 \pm 4.70)\ \Omega] > [Co(bpy)_3]^{2+/3+}$ $[33.10(34.62 \pm 1.49)\ \Omega] > I^-/I_3^-$ $[29.52(31.65 \pm 1.90)\ \Omega]$ redox shuttles and are in agreement with the corresponding decreased values of J_{sc} as shown in Table 1.[41] The large resistances observed in the low-frequency region of $[Co(bpy)_3]^{2+/3+}$ $[39(38.45 \pm 1.3)\ \Omega]$ and

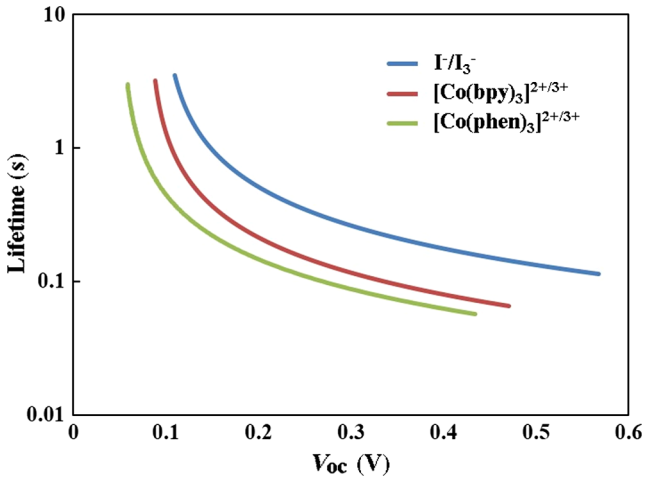

Fig. 6 Electron lifetime as a function of open circuit voltage employing cobalt- and iodine-based electrolytes.

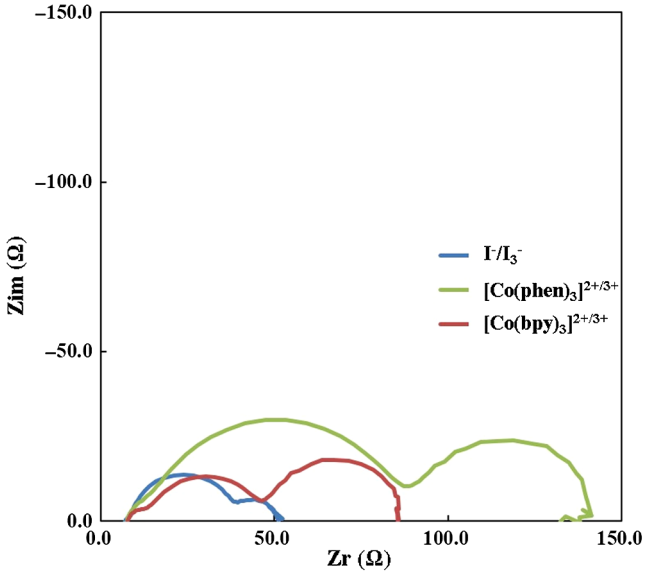

Fig. 7 Electrochemical impedance spectra of TCO-less BC-DSCs using cobalt- and iodine-based electrolytes under identical illumination condition.

Table 2 Table for EIS parameters of TCO-less BC-DSCs.

Electrolyte	$[Co(phen)_3]^{2+/3+}$	$[Co(bpy)_3]^{2+/3+}$	Iodide/tri-iodide
R_1 (Ω)	5.94 (5.1 ± 0.46)	5.87 (4.30 ± 1.35)	1.46 (1.69 ± 0.56)
R_2 (Ω)	75.53 (72.21 ± 4.70)	33.10 (34.62 ± 1.49)	29.52 (31.65 ± 1.90)
R_3 (Ω)	52.43 (59.85 ± 10.49)	39 (38.45 ± 1.3)	13.09 (12.64 ± 0.88)

The values in the bracket denote the mean value of three distinct devices along with standard deviation.

$[Co(phen)_3]^{2+/3+}$ $[52.43(59.85 \pm 10.49)\ \Omega]$-based electrolytes as compared to iodide/tri-iodide $[13.09(12.64 \pm 0.88)\ \Omega]$-based electrolyte indicate that ion diffusion is obstructed within the cobalt-based electrolytes. Consequently, sensitizer regeneration is greatly hindered for cobalt-based electrolytes, which hampers the photovoltaic behavior of the cells. The EIS results are summarized in Table 2.

Because of low cost, high flexibility, and enhanced transmittance of light in the high-wavelength region, TCO-less back contact DSC has proven to be more beneficial with respect to TCO-based DSC counterparts. Although cobalt complex-based electrolytes possess negligible optical absorption in the visible spectral range and less corrosive nature relative to the iodine-based electrolytes, they show relatively poor photovoltaic performance in BC-DSC as compared with iodine-based electrolyte, which may be due to poor dye regeneration.

4 Conclusions

Therefore, based on these findings, we performed a differential study of two most commonly utilized electrolytes (iodine- and cobalt-based redox shuttles) for the photovoltaic performance optimization of back contact TCO-less DSCs. It was observed that the use of cobalt complex-based redox mediators was hindered due to slow dye regeneration and enhanced charge transfer resistance at the TiO_2/dye/electrolyte interface and larger resistance was observed in electrolyte itself. Also this study shows the electrolyte selection criterion for photovoltaic performance enhancement in alternate DSC structure (back contact DSC) where the electrolyte travel path is higher as compared to conventional DSC architecture.

Acknowledgments

This work has been supported by the Strategic Promotion of Innovative Research and Development (S-Innovation) Program of Japan Science and Technology under the Japanese Government.

References

1. B. O'Regan and M. Grätzel, "A low-cost, high-efficiency solar cell based on dye-sensitized colloidal TiO_2 films," *Nature*, **353**, 737–740 (1991).
2. M. A. Green et al., "Solar cell efficiency tables (version 53)," *Prog. Photovoltaics: Res. Appl.* **27**(1), 2–12 (2019).
3. J. W. Lee, J. Park, and H. J. Jung, "A feasibility study on a building's window system based on dye-sensitized solar cells," *Energy Build.* **81**, 38–47 (2014).
4. L. Wei et al., "Band edge movement in dye sensitized Sm-doped TiO_2 solar cells: a study by variable temperature spectroelectrochemistry," *RSC Adv.* **5**(86), 70512–70521 (2015).
5. T. G. Ulusoy et al., "Enhanced performance of dye-sensitized solar cells by omnidirectional antireflective coatings," *J. Photonics Energy* **5**(1), 053090 (2015).
6. H. Greijer et al., "Environmental aspects of electricity generation from a nanocrystalline dye sensitized solar cell system," *Renew. Energy* **23**(1), 27–39 (2001).
7. A. K. Baranwal et al., "Tandem dye-sensitized solar cells with a back-contact bottom electrode without a transparent conductive oxide layer," *RSC Adv.* **4**(88), 47735–47742 (2014).
8. Z. Hu et al., "Transparent conductive oxide layer and hole selective layer free back-contacted hybrid perovskite solar cell," *J. Phys. Chem. C* **121**(8), 4214–4219 (2017).
9. T. Y. Tsai et al., "An efficient titanium-based photoanode for dye-sensitized solar cell under back-side illumination," *Prog. Photovoltaics: Res. Appl.* **21**(2), 226–231 (2013).
10. J. M. Kroon et al., "Nanocrystalline dye-sensitized solar cells having maximum performance," *Prog. Photovoltaics: Res. Appl.* **15**(1), 1–18 (2007).
11. N. Fuke et al., "Back contact dye-sensitized solar cells," *Jpn. J. Appl. Phys.* **46**(5L), L420 (2007).
12. N. Fuke et al., "New approach to low-cost dye-sensitized solar cells with back contact electrodes," *Chem. Mater.* **20**(15), 4974–4979 (2008).
13. D. Fu et al., "Dye-sensitized back-contact solar cells," *Adv. Mater.* **22**(38), 4270–4274 (2010).
14. D. Fu, P. Lay, and U. Bach, "TCO-free flexible monolithic back-contact dye-sensitized solar cells," *Energy Environ. Sci.* **6**(3), 824–829 (2013).
15. H. G. Yun et al., "Cost-effective dye-sensitized solar cells consisting of two metal foils instead of transparent conductive oxide glass," *Phys. Chem. Chem. Phys.* **14**(18), 6448–6451 (2012).
16. C. S. Rustomji et al., "Dye-sensitized solar cell constructed with titanium mesh and 3-D array of TiO2 nanotubes," *J. Phys. Chem. B* **114**(45), 14537–14543 (2010).
17. Y. Kashiwa, Y. Yoshida, and S. Hayase, "All-metal-electrode-type dye sensitized solar cells (transparent conductive oxide-less dye sensitized solar cell) consisting of thick and porous Ti electrode with straight pores," *Appl. Phys. Lett.* **92**(3), 033308 (2008).
18. Y. Yoshida et al., "Transparent conductive oxide layer-less dye-sensitized solar cells consisting of floating electrode with gradient TiO_x blocking layer," *Appl. Phys. Lett.* **94**(9), 68 (2009).
19. A. Hagfeldt and M. Grätzel, "Molecular photovoltaics," *Acc. Chem. Res.* **33**(5), 269–277 (2000).
20. M. Grätzel, "Conversion of sunlight to electric power by nanocrystalline dye-sensitized solar cells," *J. Photochem. Photobiol. A: Chem.* **164**(1–3), 3–14 (2004).
21. A. J. Frank, N. Kopidakis, and J. Van De Lagemaat, "Electrons in nanostructured TiO_2 solar cells: transport, recombination and photovoltaic properties," *Coord. Chem. Rev.* **248**(13–14), 1165–1179 (2004).
22. A. Islam, H. Sugihara, and H. Arakawa, "Molecular design of ruthenium (II) polypyridyl photosensitizers for efficient nanocrystalline TiO_2 solar cells," *J. Photochem. Photobiol. A: Chem.* **158**(2–3), 131–138 (2003).

23. S. Ito et al., "High-efficiency (7.2%) flexible dye-sensitized solar cells with Ti-metal substrate for nanocrystalline-TiO_2 photoanode," *Chem. Commun.*, **38**(38), 4004–4006 (2006).
24. M. J. Marchena et al., "Real-time photodynamics of squaraine-based dye-sensitized solar cells with iodide and cobalt electrolytes," *J. Phys. Chem. C* **117**(23), 11906–11919 (2013).
25. M. Z. Molla et al., "Transparent conductive oxide-less back contact dye-sensitized solar cells using cobalt electrolyte," *Prog. Photovoltaics: Res. Appl.* **23**(9), 1100–1109 (2015).
26. M. Wang et al., "Recent developments in redox electrolytes for dye-sensitized solar cells," *Energy Environ. Sci.* **5**(11), 9394–9405 (2012).
27. S. M. Feldt et al., "Design of organic dyes and cobalt polypyridine redox mediators for high-efficiency dye-sensitized solar cells," *J. Am. Chem. Soc.* **132**(46), 16714–16724 (2010).
28. Y. Liu et al., "Boosting the photocatalytic hydrogen evolution activity of gC_3N_4 nanosheets by $Cu_2(OH)_2CO_3$-modification and dye-sensitization," *Dalton Trans.* **48**(4), 1217–1225 (2019).
29. M. J. DeVries, M. J. Pellin, and J. T. Hupp, "Dye-sensitized solar cells: driving-force effects on electron recombination dynamics with cobalt-based shuttles," *Langmuir* **26**(11), 9082–9087 (2010).
30. S. M. Feldt et al., "Effects of driving forces for recombination and regeneration on the photovoltaic performance of dye-sensitized solar cells using cobalt polypyridine redox couples," *J. Phys. Chem. C* **115**(43), 21500–21507 (2011).
31. G. Sauvé et al., "High quantum yield sensitization of nanocrystalline titanium dioxide photoelectrodes with *cis*-dicyanobis (4,4′-dicarboxy-2,2′-bipyridine) osmium (II) or tris (4,4′-dicarboxy-2,2′-bipyridine) osmium (II) complexes," *J. Phys. Chem. B* **104**(15), 3488–3491 (2000).
32. S. Hattori et al., "Blue copper model complexes with distorted tetragonal geometry acting as effective electron-transfer mediators in dye-sensitized solar cells," *J. Am. Chem. Soc.* **127**(26), 9648–9654 (2005).
33. K. Kakiage et al., "Highly-efficient dye-sensitized solar cells with collaborative sensitization by silyl-anchor and carboxy-anchor dyes," *Chem. Commun.* **51**(88), 15894–15897 (2015).
34. Z. Sun, M. Liang, and J. Chen, "Kinetics of iodine-free redox shuttles in dye-sensitized solar cells: interfacial recombination and dye regeneration," *Acc. Chem. Res.* **48**(6), 1541–1550 (2015).
35. A. Zaban, M. Greenshtein, and J. Bisquert, "Determination of the electron lifetime in nanocrystalline dye solar cells by open-circuit voltage decay measurements," *ChemPhysChem* **4**(8), 859–864 (2003).
36. J. W. Ondersma and T. W. Hamann, "Measurements and modeling of recombination from nanoparticle TiO_2 electrodes," *J. Am. Chem. Soc.* **133**(21), 8264–8271 (2011).
37. T. W. Hamann and J. W. Ondersma, "Dye-sensitized solar cell redox shuttles," *Energy Environ. Sci.* **4**(2), 370–381 (2011).
38. R. Kern et al., "Modeling and interpretation of electrical impedance spectra of dye solar cells operated under open-circuit conditions," *Electrochim. Acta* **47**(26), 4213–4225 (2002).
39. J. Van de Lagemaat, N. G. Park, and A. J. Frank, "Influence of electrical potential distribution, charge transport, and recombination on the photopotential and photocurrent conversion efficiency of dye-sensitized nanocrystalline TiO_2 solar cells: a study by electrical impedance and optical modulation techniques," *J. Phys. Chem. B* **104**(9), 2044–2052 (2000).
40. M. C. Bernard et al., "Sensitization of TiO_2 by polypyridine dyes role of the electron donor," *J. Electrochem. Soc.* **150**(3), E155–E164 (2003).
41. L. Y. Lin et al., "Selective conditions for the fabrication of a flexible dye-sensitized solar cell with Ti/TiO_2 photoanode," *J. Power Sour.* **195**(13), 4344–4349 (2010).

Biographies of the authors are not available.